Contrib Mineral Petrol (2006) 152:649–665
DOI 10.1007/s00410-006-0124-1

ORIGINAL PAPER

U–Pb zircon geochronology of silicic tuffs from the Timber Mountain/Oasis Valley caldera complex, Nevada: rapid generation of large volume magmas by shallow-level remelting

Ilya N. Bindeman · Axel K. Schmitt · John W. Valley

Received: 9 January 2006 / Accepted: 16 June 2006 / Published online: 7 October 2006

Abstract Large volumes of silicic magma were produced on a very short timescale in the nested caldera complex of the SW Nevada volcanic field (SWNVF). Voluminous ash flows erupted in two paired events: Topopah Spring (TS, >1,200 km^3, 12.8 Ma)–Tiva Canyon (TC, 1,000 km^3, 12.7 Ma) and Rainier Mesa (RM, 1,200 km^3, 11.6 Ma)–Ammonia Tanks (AT, 900 km^3, 11.45 Ma; all cited ages are previously published $^{40}Ar/^{39}Ar$ sanidine ages). Within each pair, eruptions are separated by only 0.1–0.15 My and produced tuffs with contrasting isotopic values. These events represent nearly complete evacuation of sheet-like magma chambers formed in the extensional Basin and Range environment. We present ion microprobe ages from zircons in the zoned ash-flow sheets of TS, TC, RM, and AT in conjunction with $\delta^{18}O$ values of zircons and other phenocrysts, which differ dramatically among subsequently erupted units. Bulk zircons in the low-$\delta^{18}O$ AT cycle were earlier determined to exhibit ~1.5‰ core-to-rim oxygen isotope zoning; and high-spatial resolution zircon analyses by ion microprobe reveal the presence of older grains that are zoned by 0.5–2.5‰. The following U–Pb isochron ages were calculated after correcting for the initial U–Pb disequilibria: AT (zircon rims: 11.7 ± 0.2 Ma; cores: 12.0 ± 0.1 Ma); pre-AT rhyolite lava: (12.0 ± 0.3 Ma); RM: 12.4 ± 0.3); TC: (13.2 ± 0.15 Ma); TS: (13.5 ± 0.2). Average zircon crystallization ages calculated from weighted regression or cumulative averaging are older than the Ar–Ar stratigraphy, but preserve the comparably short time gaps within each of two major eruption cycles (TS/TC, RM/AT). Notably, every sample yields average zircon ages that are 0.70–0.35 Ma older than the respective Ar–Ar eruption ages. The Th/U ratio of SWNVF zircons are 0.4–4.7, higher than typically found in igneous zircons, which correlates with elevated Th/U of the whole rocks (5–16). High Th/U could be explained if uranium was preferentially removed by hydrothermal solutions or is retained in the protolith during partial melting. For low-$\delta^{18}O$ AT-cycle magmas, rim ages from unpolished zircons overlap within analytical uncertainties with the $^{40}Ar/^{39}Ar$ eruption age compared to core ages that are on average ~0.2–0.3 My older than even the age of the preceding caldera forming eruption of RM tuff. This age difference, the core-to-rim oxygen isotope zoning in AT zircons, and disequilibrium quartz–zircon and melt-zircon isotopic fractionations suggest that AT magma recycled older zircons derived from the RM and older eruptive cycles. These results suggest that the low-$\delta^{18}O$ AT magmas were generated by melting a hydrothermally-altered protolith from the same nested complex that

Communicated by T.L. Grove.

Electronic supplementary material Supplementary material is available in the online version of this article at http://dx.doi.org/10.1007/s00410-006-0124-1 and is accessible for authorized users.

I. N. Bindeman (✉)
Department of Geological Sciences, University of Oregon, Eugene, OR 97403, USA
e-mail: bindeman@uoregon.edu

A. K. Schmitt
Department of Earth and Space Sciences, UCLA, Los Angeles, CA, USA

J. W. Valley
Department of Geology and Geophysics, University of Wisconsin, Madison, WI 53706, USA

erupted high-$\delta^{18}O$ magmas of the RM cycle only 0.15 My prior to the eruption of the AT, the largest volume low-$\delta^{18}O$ magma presently known.

Keywords Paintbrush tuff · Timber Mountain tuff · Oxygen isotopes · Geochronology · Isotope zoning · Zircon · Yucca Mountain

Introduction

Isotopic zoning in phenocrysts in large silicic magma bodies

The generation and eruption of large-volume silicic magmas continue to present challenges in answering questions about size and longevity of crustal magma bodies, their physical state (e.g., stagnant, near-solidus cumulate mushes, or near-liquidus convecting liquids), and time and the depth of their segregation (e.g., Broxton et al. 1989; Bachmann and Bergantz 2003, 2004; Annen and Sparks 2002; Dufek and Bergantz 2005). Isotopic analysis of individual phenocrysts or intra-crystal domains is a novel tool to fingerprint crystal sources and to recognize separate magma batches or solid sources from which the crystals crystallized or evolved (Tepley et al. 1999; Bindeman and Valley 2001; Wolff and Ramos 2003). Many examples of isotopic zoning and disequilibria in volcanic phenocrysts have been described, and a small level of residual zoning may in fact characterize the majority of igneous rocks, even in slowly cooled plutonic examples (Tepley and Davidson 2003). The presence of isotopically zoned phenocrysts needs to be viewed as a blessing rather than a curse, because it potentially provides an important record of sources of magmas and timescales of magmatic processes. Timescales of diffusive equilibration of isotopes and trace elements are usually short (10–1,000 years) and provide a chronological resolution that is unattainable by most other methods, especially for older rocks in which U-series methods cannot be used (e.g., Bindeman et al. 2006; Costa et al. 2003). In this respect, accessory minerals with slow diffusion coefficients, and particularly zircon (Watson and Cherniak 1997; Valley 2003) are valuable probes of transient changes by diffusion and solution reprecipitation at high magmatic temperatures. Additionally, zircon is enriched in U and Th, whose radioactive decay is used widely as chronometer. The focus of the present paper is zircon U–Pb geochronology in combination with oxygen isotopic heterogeneity to deduce the genesis of large volume silicic magmas erupted from the Timber Mountain/Oasis Valley caldera complex.

Lessons from Yellowstone

Insights from studies of voluminous volcanism at Yellowstone (Hildreth at al. 1984; 1991; Bindeman and Valley 2001; Bindeman et al. 2001; Vazquez and Reid 2002) provide guidance for the evaluation of oxygen isotopic data from the SWNVF earlier described by Bindeman and Valley (2003). Low-$\delta^{18}O$ magmas of Yellowstone bear clear evidence that they were generated at very shallow crustal levels by remelting of hydrothermally-altered volcanic caldera-fill of the previous magmatic cycles. This interpretation is based on the discovery of inherited high-$\delta^{18}O$ cores in quartz and zircon crystals and the ages of zircons in low-$\delta^{18}O$ units that show a predominance of pre-eruptive zircon ages similar to those from the stratigraphically lowest caldera-forming tuff—the ~2 Ma Huckleberry Ridge tuff (Bindeman et al. 2001). It is important to stress that the highly radiogenic isotopic ratios of Sr, Nd, and Pb of all Yellowstone rhyolites and basalts are consistent with assimilation of the Archean crust of the Wyoming block (Hildreth et al. 1991; Vazquez and Reid 2002). However, no Archean zircon xenocrysts and only three Cretaceous and Triassic xenocrysts were present among > 200 individual zircons analyzed in studies of Bindeman et al. (2001) and Vazquez and Reid (2002). The majority of xenocrysts were of Pleistocene to Late Oligocene age, consistent with the age of Yellowstone volcanism. Bindeman and Valley (2001) and Bindeman et al. (2001) estimated that more than 50% of dated zircon cores, including cores in the isotopically-zoned smallest zircon (50–70 μm) were inherited. The timescale of generation of ~40 km^3 of most $\delta^{18}O$-depleted rhyolites is constrained by partial isotopic annealing and overgrowth of zircon and quartz and implies that significant volumes (tens of km^3) of rhyolite magma were generated by bulk remelting within 500–5,000 years and at very shallow crustal levels (Bindeman and Valley 2001). Vazquez and Reid (2002) used U–Th disequilibrium methods to date zircons in younger, less $\delta^{18}O$-depleted intracaldera rhyolites that lack isotopic zoning and disequilibrium with other mineral phases. They found fewer, yet > 10%, inherited zircons but inferred a protracted residence of zircons in a crystal mush, rather than remelting.

Recently, Boroughs et al. (2005) presented phenocryst evidence that many voluminous older tuffs (10–12 Ma) along the Yellowstone hot spot track are $\delta^{18}O$-depleted, thus significantly expanding the number of known low-$\delta^{18}O$ magmas. However, these authors

interpreted the origin of these rhyolites as a result of remelting of the Cretaceous Idaho batholith. This interpretation, versus volcanic cannibalism of the pre-existing volcanic pile is pending confirmation from dating zircons and determining their $\delta^{18}O$ values.

Timber Mountain/Oasis Valley Caldera Complex

The voluminous volcanic rocks of the SWNVF provide the second best example after Yellowstone of shallow level volcanic cannibalization of rocks from the previous volcanic activity in the area.

The magmatic activity in the SWNVF, one of the largest centers of silicic magmatism in the western USA, extended from ~16 to <9 Ma (Fig. 1). The present work focuses on the voluminous ''ignimbrite flare-up'' in the SWNVF that happened between 13 and 11 Ma, generated >4,000 km^3 of silicic magma, and led to the formation of four major overlapping calderas (Christiansen et al. 1977; Byers et al. 1989). From a plate-tectonic perspective, SWNVF is a part of the 37–5 Ma volcanism in the Southern Basin and Range, which has been related to subduction of the Farallon Plate and subsequent regional extensional tectonism in the Great Basin (Lipman et al. 1972; Eaton 1984). A remarkable feature of SWNVF magmatism is that some tuffs are depleted in $^{18}O/^{16}O$ ratio with respect to their preceding higher-$\delta^{18}O$ tuffs (Friedman et al. 1974; Lipman and Friedman 1975), while others are enriched in $\delta^{18}O$. The >1,000 km^3 Ammonia Tanks (AT) cycle (AT tuff, pre-AT and post-AT lavas) is the largest-volume, single, low-$\delta^{18}O$ magmatic unit known, with $\delta^{18}O$ values of minerals and calculated melt one to 1.5‰ lower than the mantle.

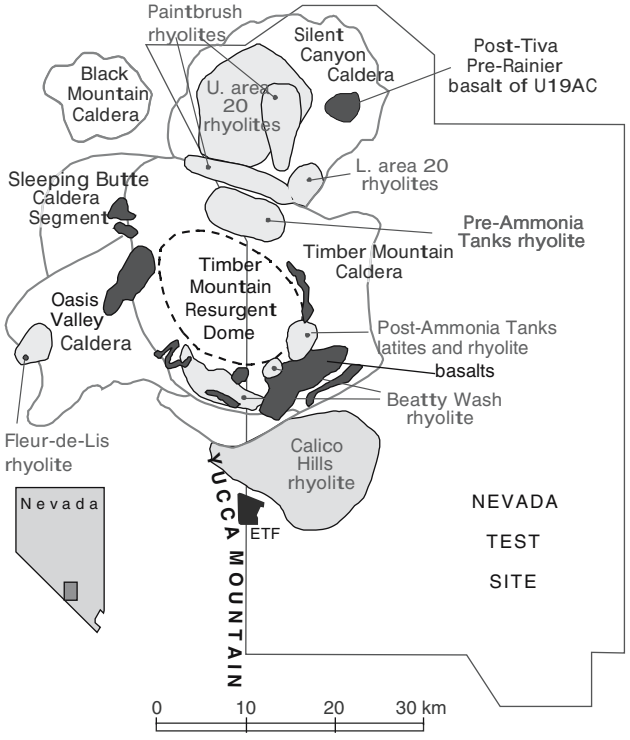

Fig. 1 Map of the Timber Mountain/Oasis Valley caldera complex of South Western Nevada Volcanic field (SWNVF). Caldera rims for the four ash-flow sheets overlap. Eruptions of Paintbrush Group (Topopah Spring, Tiva Canyon tuffs, 12.8–12.7 Ma, > 2,200 km^3), and Timber Mountain Group (Rainier Mesa and Ammonia Tanks tuffs, 11.6–11.45 Ma, > 2,200 km^3) resulted in formation of Oasis Valley and Timber Mountain Calderas, respectively (Byers et al. 1976a, b; Christiansen et al. 1977). Smaller volume rhyolitic and basaltic (*unmarked darker grey*) lavas erupted following caldera collapses. Yucca Mountain is made of Topopah Spring and Tiva Canyon tuffs. Exploratory tunnel facility (ETF) for long-term storage of nuclear waste is shown

The >1,000 km^3 Ammonia Tanks (AT) cycle (AT tuff, pre-AT and post-AT lavas) is the largest-volume, single, low-$\delta^{18}O$ magmatic unit known, with $\delta^{18}O$ values of minerals and calculated melt one to 1.5‰ lower than the mantle.

Repeated eruption of voluminous ignimbrites over a ~7 Ma time-span resulted in a group of nested calderas within the same lithospheric block of late Proterozoic to Paleozoic metasedimentary rocks overlying Precambrian basement (Christiansen et al. 1977; Byers et al. 1989). In general, the 16–13 Ma silicic volcanics are less exposed because they are overlain by younger tuffs and lavas. Compositionally-zoned silicic ash flow sheets of Paintbrush (12.8–12.7 Ma) and Timber Mountain (11.6–11.45 Ma) groups are the most voluminous and regionally abundant units and they are the primary focus of this paper. Paintbrush Group tuffs: Topopah Spring (TS, > 1,200 km^3, 12.8 Ma), Tiva Canyon (TC, 1,000 km^3, 12.7 Ma); and Timber Mountain Group tuffs: Rainier Mesa (RM, 1,200 km^3, 11.6 Ma), and Ammonia Tanks (AT, 900 km^3, 11.45 Ma) are related to four major caldera-forming events in the same general area (Fig. 1). Significantly, the $^{40}Ar/^{39}Ar$ ages of sanidine in each tuff unit (Sawyer et al. 1994; Huysken et al. 1994, 2001) demonstrate that only 100 k.y. separate TS from TC, and 150 k.y. separate RM from AT, two subsequent caldera-forming eruptions within the Paintbrush and Timber Mountain cycles, respectively. Additionally, smaller volume (~40 km^3) tuffs, such as Pah Canyon, are present in between these TS and TC ignimbrite units (Flood et al. 1989). These relatively short time intervals between large volume eruptions are critical constraints for understanding the petrogenesis of these magmas. Table 1 summarizes mineralogical and chemical composition of samples studied in this paper. A majority of the samples for this study comes from within the Nevada Test Site or Yucca Mountain, where TS and TC tuffs make the bulk of the proposed US nuclear waste repository.

Each of these four ash-flow sheets (here called tuffs for brevity) is zoned in composition and phenocryst

Table 1 Summary of petrologic and isotopic parameters of analyzed samples

Sample ident	Unit	Phenocrysts		SiO_2 (%)	$\Delta^{18}O$, T °C			TZrc (°C)	$\delta^{18}O$ melt	ϵNd	$^{87}Sr/^{86}Sr_I$
		Vol%	Abundance		Qz-Mt	San-Mt	Mt-Ilm				
Topopah spring tuff, > 1,200 km^3, 12.8 Ma											
TM-10	TS, upper	16	PSQBHCSpZMI	67.3	872	965	978	896	8.06	–10.6	0.7150
Tiva canyon tuff, 1,000 km3, 12.7 Ma											
TM-12	TC, upper	11	PSBHCSpZMI	67.0		970	838	852	7.25	–10.77	0.7088
Rainier mesa tuff, 1,200 km3, 11.6 Ma											
TM-16	RM, upper	23	PSQBHCSpZMIO	76.8	748	711	718	797	8.13	–10.45	0.70843
Pre-ammonia Tanks rhyolite											
TM-24	pre-AT	7	SPQHCSpZMI	75.5	754	744	710	776	5.73		0.71358
Ammonia tanks tuff, 900 km3, 11.45 Ma											
TM-15	AT, lower	14	SQPBHCSpZMI	75.7	762	766	662	809	5.57	–10.3	0.7150
TM-17	AT, upper	19	PSQBHCSpZMI	73.1	870	899	816	842	5.39	–9.45	0.7078
Post-ammonia Tanks rhyolite											
TM-21		20	PSQBHCSpZMI	74	784			795	5.45	–9.64	0.70776

P plagioclase, *S* sanidine, *Q* quartz, *B* biotite, *H* hornblend, *C* clinopyroxene, *sp* sphene, *Z* zircon, *M* magnetite, *I* ilmenite

Oxygen isotopic values for melt are calculated from phenocrysts (Bindeman and Valley 2003); Nd and Sr analyses are from Farmer et al. (1991)

content, with smaller-volume crystal-rich (15–25%) upper latitic (or even more mafic) portions residing on top of voluminous crystal-poor (1–15%) lower rhyolitic portions (Table 1, Warren et al. 1989). Such stratigraphic sequences are traditionally interpreted to represent inverted stratigraphy of the magma chamber, implying that the position of latites and rhyolites was reversed in the magma chamber prior to eruption (e.g., Lipman 1984). Pumice clast compositions, and Fe–Ti oxide equilibration temperatures vary continuously in each tuff unit (Lipman et al. 1966, Lipman 1971; Flood et al. 1989; Mills et al. 1997), and reflect compositional and temperature zoning in pre-climactic magma chambers. Study of melt inclusions in sanidine and quartz phenocrysts in rhyolitic and latitic portions of TS, RM and AT tuffs (Vogel and Aines 1996) demonstrates that volatile content increased upward (towards the rhyolites) in magma chambers. Despite wide variations in composition and temperature in each tuff unit, there is a small compositional gap at ~65 wt% SiO_2 (Mills et al. 1997) separating rhyodacitic to high-silica rhyolitic (~67–76 wt% SiO_2), and basaltic to latitic chemical groups (53–65 wt% SiO_2), although mafic pumices are rare (Schuraytz et al. 1989; Flood et al. 1989; Warren et al. 1989, 2000).

Oxygen isotope zoning in zircons

In an attempt to find oxygen isotope zoning similar to that in Yellowstone (Bindeman and Valley 2001), zircons from Timber Mt tuffs were separated into size fractions. Oxygen isotope analyses were performed by laser fluorination of: bulk, smaller (<53 μm in diameter), and larger (>105 μm, >149 μm) size fractions, and air-abraded cores of large zircons. Rhyolitic and latitic portions of normal- to high-$\delta^{18}O$ TS, TC, and RM tuffs exhibit no difference between large and small zircons, or zircon cores retrieved by air-abrasion (Fig. 2), and their $\delta^{18}O$ values are in equilibrium with those of other minerals for the same tuffs. However, low-$\delta^{18}O$ rocks of the AT cycle—pre-AT rhyolitic lava, rhyolitic and latitic portions of AT tuff, and post-AT crystal-rich latitic lava, (Table 1) exhibit evidence of isotopic zoning. Air-abraded cores of larger (> 105 μm diameter) zircons are consistently 0.4–0.5‰ higher in $\delta^{18}O$ than smaller (< 53 μm) zircons in three samples (Bindeman and Valley 2003). These differences exceed analytical uncertainty (± 2 standard deviations of replicate measurements < 0.2‰) and suggest 1.5–2‰ $\delta^{18}O$ zoning in AT zircons when compared to the calculated curves based on diffusion modeling calculations (Fig. 3). Similar zoning would be inferred if low $\delta^{18}O$ rims formed as new zircon overgrowths.

Additionally, $\Delta^{18}O$(Qz–Zrc) for these samples is 1.6–1.8‰, while $\Delta^{18}O$(melt-Zrc cores) is 0.6–0.9‰ (Fig. 2b), which is 0.5–0.9‰ smaller than the expected $\Delta^{18}O$(Qz–Zrc) equilibrium values between 750° and 850°C (2.5–2.1‰, Valley et al. 2003). Even smaller (<53 μm) zircons show somewhat lower differences in $\Delta^{18}O$(Qz–Zrc) and $\Delta^{18}O$(melt-Zrc), although they are closer to equilibrium. The $\Delta^{18}O$(Qz–Zrc) and $\Delta^{18}O$(melt-Zrc) disequilibria are a direct result of isotopic zonation of zircon where elevated $\delta^{18}O$ is preserved in zircon cores, because quartz is in equilibrium

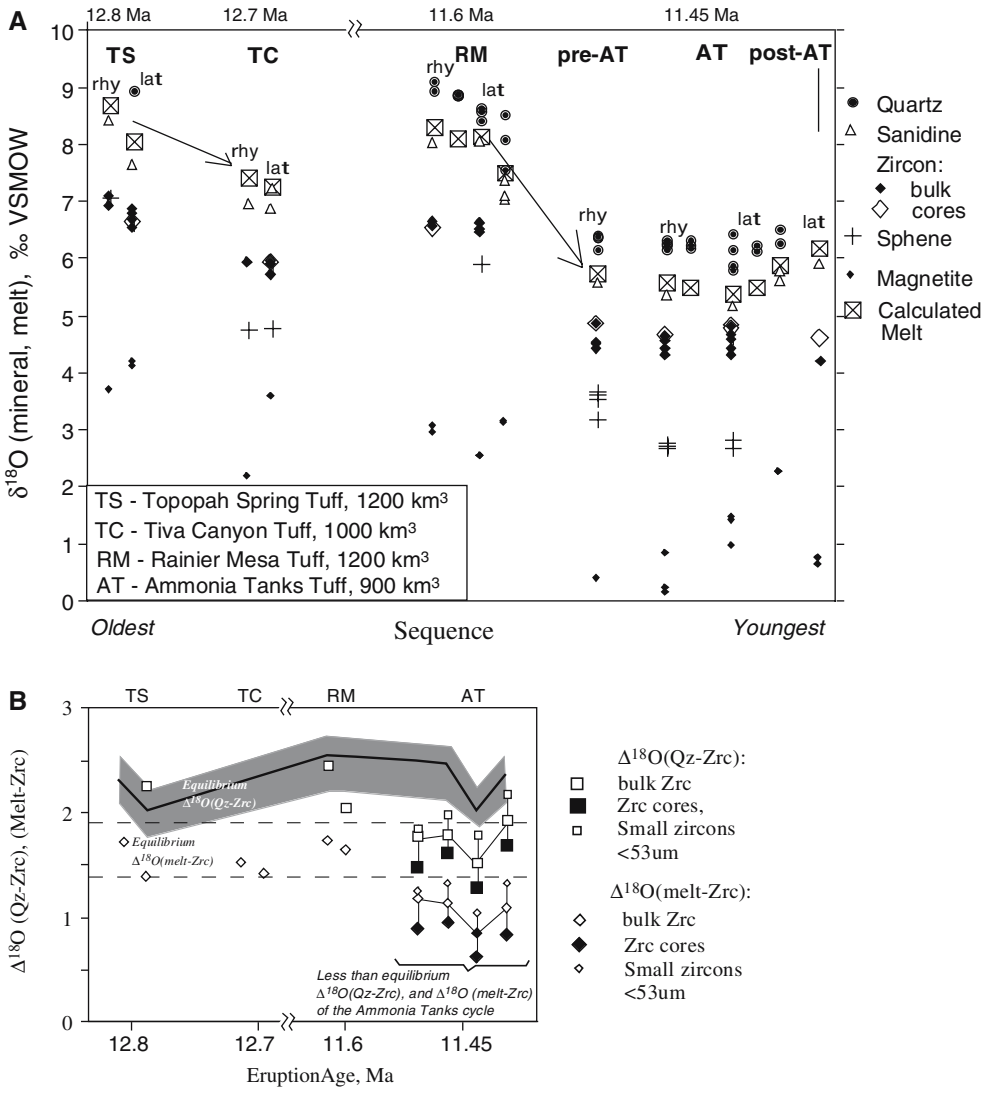

Fig. 2 **a** Evolution of $\delta^{18}O$ in minerals (measured) and melt (calculated) of four major tuffs and two lavas from SWNVF (data are from Bindeman and Valley 2003). Notice sudden depletion of $\delta^{18}O$ after TS and RM. AT represents a low-$\delta^{18}O$ magma. First column(s) of each unit is rhyolite, second is latite; there are two samples of latite and rhyolite in RM, and two samples of rhyolite and three samples of latite in AT. Notice smaller mineral-mineral isotopic fractionation in latites as compared to rhyolites due to higher temperature of the former. Air-abraded cores of zircons are higher in $\delta^{18}O$ than bulk zircons or smaller zircons in AT tuffs, pre-AT, and post-AT lavas. **b** Isotope fractionations between zircons and quartz, and zircon and melt. Calculated Quartz–Zircon values are based on $\Delta^{18}O$(Quartz-Mt) temperatures from Table 1, with envelope showing a range of ± 50°C, and A factor $\Delta^{18}O$(Quartz-Zrc) of 2.64 (Valley et al. 2003). Values of $\Delta^{18}O$(Melt-Zircon) of 1.4‰ (latites, 870°C) and 1.9‰ (rhyolites, 750°C) correspond to equilibrium values at respective melt compositions and temperatures as measured in Bishop tuff (Bindeman and Valley 2002). Notice that zircons in all four of Ammonia Tanks cycle samples have smaller than equilibrium fractionations vs. quartz, due to the inherited high-$\delta^{18}O$ cores which are present even in smaller zircons

with the melt and other minerals (Bindeman and Valley 2003). The discovery of oxygen isotope zoning in zircons from low-$\delta^{18}O$ tuff and lavas of SWNVF, second to Yellowstone, is a significant result.

Samples and procedure

Samples selected for U–Pb age analysis are described in detail by Bindeman and Valley (2003) and references therein, and are briefly characterized in Table 1. One sample of each TS, TC, and RM tuff was selected for high spatial resolution U–Pb zircon dating, along with three samples of the younger AT cycle: samples TM-15 and TM-17, for lower and upper AT tuff, respectively, and one precursor rhyolitic lava—TM-24. Zircons were separated from crushed and sieved rocks using standard heavy liquid separation techniques. Additionally, zircons were extracted by dissolving

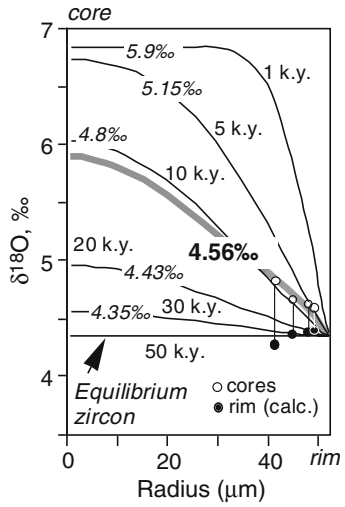

Fig. 3 Oxygen isotope zoning profile through zircons in Ammonia Tanks tuff, and results of diffusion modeling for post crystallization exchange. The calculated equilibration time (k.y.) using diffusion coefficient for water-saturated oxygen diffusion at 850°C from Watson and Cherniak (1997), solved numerically for diffusion in a sphere using Crank (1975), see Bindeman and Valley (2001, 2003) for analytical data and details of calculations. Similar conclusions will result if zircon rims grew as new overgrowths. The value 4.56‰ is the measured bulk $\delta^{18}O$ of zircons; *smaller italic values* are calculated bulk composition for each shown zoning profile. *Thin vertical lines* connecting *open* and *closed circles* are located at distances removed by air abrasion. *Open circles* (cores) represent measured values of the remaining material after each step of air abrasion of the same population calculated from the mass (volume) of material remaining relative to the initial mass; *closed symbols* are calculated $\delta^{18}O$ values based on the measured core values, initial sample $\delta^{18}O$ value, and mass of zircon remaining. *Thick line* represents a profile drawn through the population

phenocryst-free glass shards of samples TM-15 and TM-17 in order to avoid any zircons included in phenocrysts. No difference in age between zircons extracted from bulk samples or by HF-dissolution of glass was found. Thus, HF-extracted zircons are discussed together with their parental samples.

Typically, 30–40 zircon grains per sample were hand-picked, mounted in epoxy, polished to ~75 % of their midsection, and mapped in reflected light and back-scattered electron imaging. Analyses of U–Pb age were performed using the UCLA Cameca 1270 ion microprobe using standard protocols for the analysis of youthful zircons (Schmitt et al. 2003a). Ion intensities were measured in 12–15 cycles using a mass-filtered O^- primary ion beam of ~15 nA focused to an oval 25–30 μm spot. AS-3 (Paces and Miller 1993) and 91,500 (Wiedenbeck et al. 1995, 2004) reference zircons were used to calibrate U, Th, and Pb sensitivities, following the technique of Compston et al. (1984). The analytical procedure included initial scanning ion microscopic imaging of UO^+ in order to identify comparatively U-rich grains. These grains were then chosen for subsequent analysis. In addition to analysis of polished grains, unbroken, euhedral zircon crystals were placed flush on sticky-tape and mounted in epoxy. The crystal growth faces of these grains were analyzed without polishing to determine rim compositions. From depth profiling of the sputter pits (using a DEKTAK surface profilometer), we estimate that each ''rim'' analysis sampled the outermost ~0.3 to ~1.5 μm margins of the grains, which allows a linear spatial resolution that is one order of magnitude smaller perpendicular to the crystal face than by conventional spot analysis. Note that precleaning of the surface and stabilization of the secondary ion signal prevented the use of the first ~200 s of the analysis, which removed ~0.3 μm of each zircon. Subsequently, grains were ground twice at depth intervals of ~5 μm, and a new analysis spot was placed directly below the remaining 0–1 μm-deep pit. Using this technique, ages have been determined for one grain (TM17-Mount 2-g3) at ~0, 5, and finally 10 μm depth. The reproducibility of U-Pb sensitivity factor based on the age reproducibility of reference

Table 2 Summary of U-Pb ages of zircons in studied units of SWNVF

Unit	Eruption age, (Ma)	Zircons analyzed	Spots analyzed	Xenocrysts	U-Pb age[a] (Ma)	± 1σ[c]	MSWD	U-Pb age[b] accepted	±1σ[c]	MSWD
Ammonia Tanks (rims)	11.45	5	9	0	11.63	0.18	1.20	11.73	0.20	2.39
Ammonia Tanks (cores)	11.45	27	30	0	11.85	0.17	1.07	11.97	0.14	1.18
pre-AT rhyolite	11.6–11.45	10	10	0	11.76	0.27	2.87	11.95	0.30	5.35
Rainier Mesa	11.6	10	10	1	12.12	0.35	4.82	12.35	0.30	5.19
Tiva Canyon	12.7	10	11	0	13.19	0.18	1.33	13.18	0.15	1.38
Topopah Spring	12.8	10	10	0	13.41	0.23	0.64	13.45	0.23	0.64

Euption age is Ar-Ar sanidine ages from Sawyer et al. (1994)

[a] Weighted average of individual ^{207}Pb-corrected and disequilibrium corrected ages

[b] Errors multiplied with square-root of MSWD if MSWD > 1

[c] Concordia intercept age from regression through $^{207}Pb/^{206}Pb = 0.8283$

zircon AS3 during the four days of data acquisition was as follows (all values 1 standard deviation): 4.9% (December 20, 2004, $n = 10$), 1.4% (December 21, 2004, $n = 9$), 2.8% (December 22, 2004, $n = 11$), and 1.3% (December 23, 2004, $n = 9$).

We have also measured core and rim oxygen isotopic ratio of eight mounted and polished zircons from the Ammonia Tanks tuff at the University of Wisconsin-Madison on a CAMECA 1280 ion microprobe using a Cs primary beam using KIM-5 zircon standard (Valley et al. 2005); analytical details will be reported in detail elsewhere.

Results

U–Pb ages of major tuff units

Figure 4 and Table 2 presents U–Pb ages of zircon populations in four tuffs from caldera-forming eruptions and one precursor lava (TM-24) with MSWD values and individual uncertainties, individual analyses are given in the Appendix. Unlike the U-rich Yellowstone zircons, which crystallized from intraplate magma with high HFSE, and high U and Th magmas, the subduction-related magmas of the SWNVF are HFSE-depleted and thus U-poorer, but have Th/U values highest than that measured for other igneous zircons worldwide, see below. Consequently, U abundances of the analyzed zircons are on average only ~100 ppm, with somewhat higher abundances in RM (~400 ppm) and pre-AT rhyolite (~700 ppm). This results in relatively low radiogenic ^{206}Pb yields (on average ~95%) that limits analytical precision: only ~55% of the analyses have $^{206}Pb/^{238}U$ age uncertainties that are within the ~2 to 5% analytical uncertainty that can be achieved for grains with high radiogenic ^{206}Pb yield (>99%).

After correcting for the initial U–Th disequilibrium (Schärer 1984, Wendt and Carl 1985), the following U–Pb isochron ages were obtained using the fixed-intercept regression method of Mahon (1996): AT (rims 11.73 ± 0.20 Ma, MSWD = 2.4; cores 11.97 ± 0.14 Ma, MSWD = 1.2; pre-AT rhyolite lava 11.95 ± 0.30 Ma, MSWD = 5.3; RM 12.35 ± 0.30, MSWD = 5.19; TC 13.18 ± 0.15 Ma, MSWD = 1.38; TS 13.45 ± 0.23, MSWD = 0.64. Individual zircon $^{206}Pb/^{238}U$ model ages were calculated using a ^{207}Pb-based common Pb correction and are plotted in Fig. 4 as cumulative probability curves and individually in Fig. 4. The following observations result from inspection of our data.

1. Both, the isochron and cumulative population ages show short time gaps between TS and TC, and RM and AT units, comparable to the Ar–Ar stratigraphy for these tuff units (Sawyer et al. 1994; Huysken et al. 2001). This independent geochronologic result confirms the outstanding feature of the SWNVF—that large volume silicic magmas were rapidly generated and erupted from the same nested caldera complex on timescales of 10^4–10^5 years.
2. Xenocrysts older than the age of initiation of volcanism at Timber Mt. are lacking, except for a single zircon of Proterozoic age. This result adds to

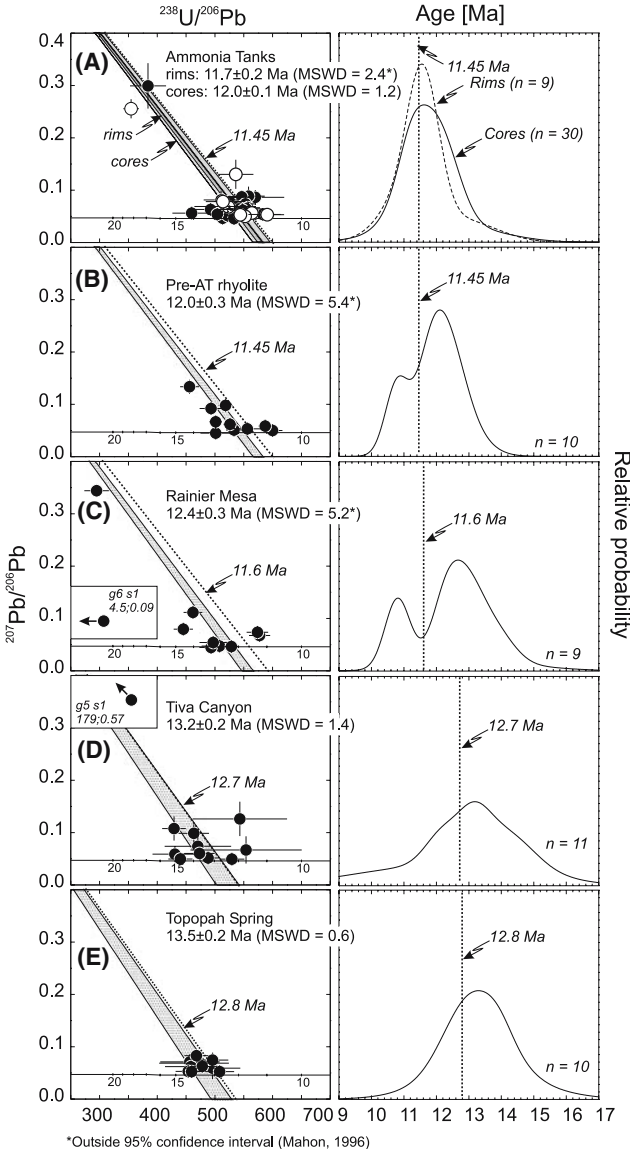

Fig. 4 Tera-Wasserburg Concordia diagrams showing ages of four major caldera-forming tuffs (**a**, **c**, **d**, **e**), and one precursor lava (**b**). Panels on right show cumulative probability curves of ^{207}Pb-corrected $^{206}Pb/^{238}U$ zircon ages of the same analyses

the growing database of individual zircon U–Pb dates in different magmatic environments, showing surprising rarity of xenocrysts that predate the initiation of magmatic activity (Lowenstern et al. 2000; Bindeman et al. 2001; Vazquez and Reid 2002; Schmitt et al. 2003a, b; Simon et al. 2005; Charlier et al. 2003; Bacon and Lowenstern 2005).

3. The average U–Pb ages in each of the five analyzed samples are 0.7–0.35 Ma older than their respective Ar–Ar eruption ages; ages of zircon populations in TC and AT units are coeval or even older than Ar–Ar ages of the preceding units of the same cycle, TS and RM respectively. Collectively, zircons in the TC, and AT, and pre-AT units not only predate the Ar–Ar age of the caldera formation, but also that of the preceding volcanic cycle.
4. Zircons in three samples of the last, low-δ^{18}O AT volcanic cycle, one sample of the precursor rhyolitic lava, and samples of early and late-erupted tuffs have overlapping U–Pb ages, which are collectively older than the Ar–Ar sanidine eruption age of the AT tuffs. At the same time, U–Pb ages of zircon rims in AT cycle (11.7 ± 0.2 Ma) are closer to the Ar–Ar sanidine age (11.45 ± 0.07 Ma, Sawyer et al. 1994) and agree with it within two sigma errors. We explore these results in greater detail below.

U–Pb ages of low-δ^{18}O magmas of AT cycle with δ^{18}O-zoned zircons

A total of 30 spot analyses on individual zircons from the AT cycle were performed and the data are plotted in Fig. 5. The relatively large uncertainties of many individual analyses, and the short time intervals between successive caldera-forming eruptions makes it very difficult to resolve the origin of individual zircons in the AT magmas as being derived from each preceding particular tuff unit, nor does the ion microprobe depth profiling for a single grain TM17-Mount 2-g3 (Table 1) resolve a significant age increase toward the core. We notice, however, that nine rim ages are collectively on average younger than core ages. If we only include analyses that have radiogenic yields >99%, then average rim and core ages for AT zircons are different by ~600,000 years, with the rim ages essentially indistinguishable from the Ar–Ar eruption age (AT cores 12.1 ± 0.2 Ma, MSWD = 1.8, n = 7; AT rims 11.5 ± 0.2 Ma, MSWD = 0.6, n = 5). In summary, there are indications for a heterogeneous AT zircon population, with a significant portion being older than even the age of the preceding caldera-forming eruption of the RM tuff. This result is supported by the δ^{18}O zircon zoning of the same zircon population (Fig. 2), performed by air abrasion, and by individual SIMS analyses below, which shows 1.5‰ core to rim zoning (Fig. 2). Therefore, the older age, and the presence of higher-δ^{18}O zircon cores are discussed in conjunction.

δ^{18}O values of individual zircons in the AT magmas

SIMS analyses of eight individual zircons in two AT samples (TM15 and TM17) confirm 0.5–2.6‰ core-to-rim δ^{18}O zoning within four individual zircons, while the other four zircons exhibit more subdued zoning (Table 3; Fig. 6). Zircon cores span the range from 7.1 to 3.9‰, and the average value of eight core analyses is 4.9‰, or 0.2–0.3‰ higher than the average laser analysis of bulk cores retrieved by air abrasion of large zircon crystals (Bindeman and Valley 2003; Fig. 3). At the same time, the average composition of zircon rim analyses of this study is 4.02 ± 0.33‰ (1 standard deviation on 12 analyses); this value is 0.3‰ lower than one estimated based on mass-balance during the successive air abrasion of fractions of large zircons (Fig. 3). Therefore, due to higher spatial resolution of the 10 μm spot ion microprobe analysis, larger average core-to-rim zoning is observed, and a more complex individual zircon δ^{18}O zoning is found that may have formed by a combination of oxygen diffusion through early formed zircon and overgrowths of new zircon. More importantly, SIMS analysis of eight individual

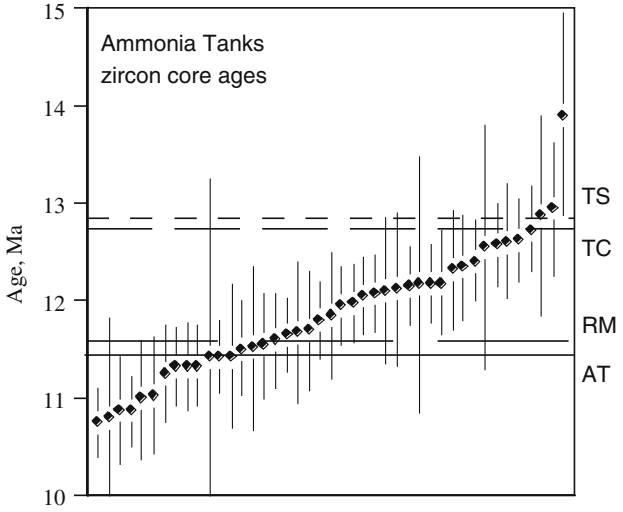

Fig. 5 Zircon ages with uncertainties in the Ammonia Tanks cycle magmas that extend the entire history of magmatism in Timber Mountain Caldera Complex, SWNVF; *horizontal lines* denote Ar–Ar sanidine ages of caldera-forming eruptions (Sawyer et al. 1994)

zircons yielded two high-$\delta^{18}O$ zircon cores, characteristic of older eruption units.

Th/U ratios of Timber Mountain zircons

Compared to zircons from other silicic igneous systems, the Timber Mountain zircons have much higher Th/U ratios between ~0.4 and 4.7 (Fig. 7). This range exceeds the ''canonical'' range for igneous zircon of 0.1–0.5, for which exceptions are only stated for mantle xenoliths (Th/U ~0.2–1.0) or carbonatitic zircons (Th/U up to 9,000; all values cited from the compilation by Hoskin and Schaltegger 2003). In order to address this issue in greater detail, we compiled Th/U for magmatic zircons from a range of compositions. Felsic compositions are dominantly for Cenozoic volcanic suites from the Western USA, and mafic compositions include Proterozoic Duluth gabbro, Proterozoic anorthosites, and Miocene MORB gabbros/diorites (Fig. 7 and references therein). This compilation corroborates the result of Hoskin and Schaltegger (2003) that most igneous zircons have Th/U ~ 0.5 with a range from ~0.2 to ~0.9), and therefore the exceptionally elevated Th/U of Timber Mountain zircons warrant special discussion. Also indicated on Fig. 7 are $D_{Th/U}$ (ratio of the mineral/melt partitioning coefficients for Th over U) that were calculated from average Th/U of the whole-rock samples used in the compilation of zircon Th/U data. While the uncertainties for $D_{Th/U}$ are relatively large due to the observed spread in zircon Th/U, it is remarkable that $D_{Th/U}$ is rather constant for the entire compositional range taken into consideration, including the Timber Mountain suite. The average $D_{Th/U}$ of ~0.2 that we obtained for a wide compositional range is comparable to the $D_{Th/U}$ ~0.17 measured by Hinton et al. (cited as written communication in Blundy and Wood 2003). We find that elevated Th/U in Timber Mountain zircons are thus inherited from their high Th/U magmas, the significance of which is discussed below.

Table 3 SIMS analyses of individual zircons for oxygen isotopic ratios; uncertainty is based on eight KIM5 zircon standards analyzed before and after these analyses

Crystal-spot (core, rim)	U-Pb core age	± 1SD
Sample TM-15, Ammonia Tanks tuff, lower		
TM15-1-1c	5.79	0.18
TM15-1-2r	4.09	0.18
TM15-1-3c/r	4.59	0.18
TM15-1-4r	3.37	0.18
TM15-2-1c	4.59	0.18
TM15-2-2r	4.01	0.18
TM15-2-3r	4.17	0.18
TM15-2-4r	3.91	0.18
TM15-3-1c	4.50	0.18
TM15-3-2r	4.60	0.18
TM15-4-1c	4.30	0.18
TM15-4-2r	4.17	0.18
TM15-5-1r	3.74	0.18
TM15-5-2r	3.78	0.18
TM15-5-3c	3.88	0.18
TM15-6-1r	3.86	0.18
TM15-6-2c	4.45	0.18
Sample TM-17, Ammonia Tanks tuff, upper		
TM17-4-1c	7.05	0.18
TM17-4-2r	4.45	0.18
TM17-3-1r	4.15	0.18
TM17-3-2c	4.60	0.18

Crystal size distribution of zircon and quartz

In an additional attempt to find textural evidence for zircon inheritance in AT magmas, we measured crystal size distribution and volume abundance of zircon and quartz (Fig. 8, Table 4) following dissolution and measurement techniques described in Bindeman (2003). The motivation in this effort was to find distinctive features indicating inheritance in the shapes of CSD graphs. Figure 8 shows that the CSD of each

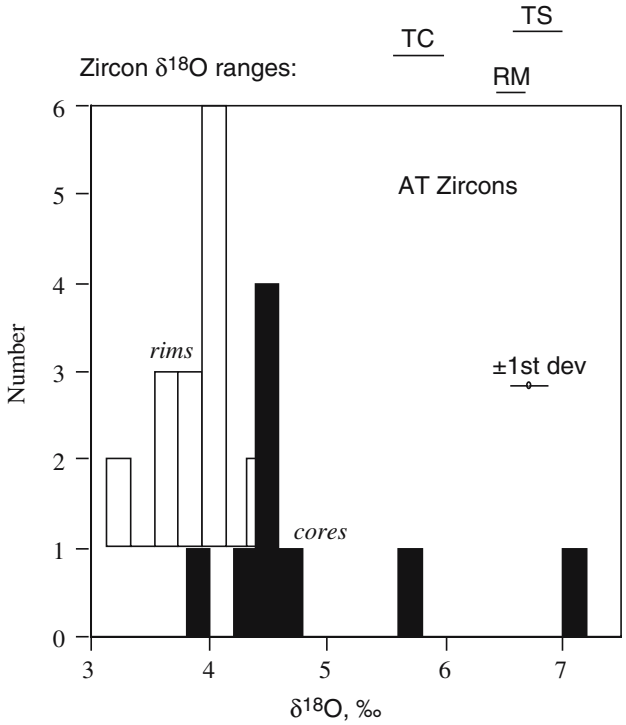

Fig. 6 Oxygen isotope ratios in individual zircons from the Ammonia Tanks magmas. Histograms of cores and rims are based on 21 analyses of eight crystals (Table 3); Individual analyses have $\delta^{18}O$ uncertainty of ± 0.18‰ (1 SD), based on the block of eight KIM-5 zircon standards mounted and analyzed together with the AT zircons

sample defines a unique pattern with progression toward larger crystals with greater abundance of crystals per volume of magma from precaldera to postcaldera magmas of the AT cycle. Notably, CSDs for zircon and quartz share the same overall lognormal pattern, similar to other silicic extrusive rocks (Poldervaart 1956; Bindeman 2003). The CSD of zircon in the RM tuffs is similar in shape and mode of maximum abundance, but lower in concentration, than zircons in the upper and lower AT tuffs. The pre-AT lava is however distinct in having fewer and smaller zircons (Table 4, Fig. 8), and quartz, while postcaldera AT lava has the largest quartz (Table 4). These features are easily interpreted as reflecting the progress of zircon and quartz crystallization from earlier to later units. Although there are some hints of inheritance in the CSD zircon pattern – the pre-AT lava TM-24 has a distinct bend at ~100 μm zircons showing larger proportion of large grains than is typical for crystallization, the inherited zircon population in subsequent AT tuffs is texturally blended with newly crystallized, and overgrown grains. The same conclusion was reached in comparing CSD of zircons from the Deadman Creek dome in Long Valley caldera that were dated by the ion microprobe (Bindeman 2003): while these zircons showed significant inheritance (Reid et al. 1997), post inheritance recrystallization modified the zircon CSD. It should also be pointed out that slopes of the CSD of both quartz and zircons vary insignificantly (e.g. < 2 ×), and we do not interpret these slopes as reflecting crystal residence times.

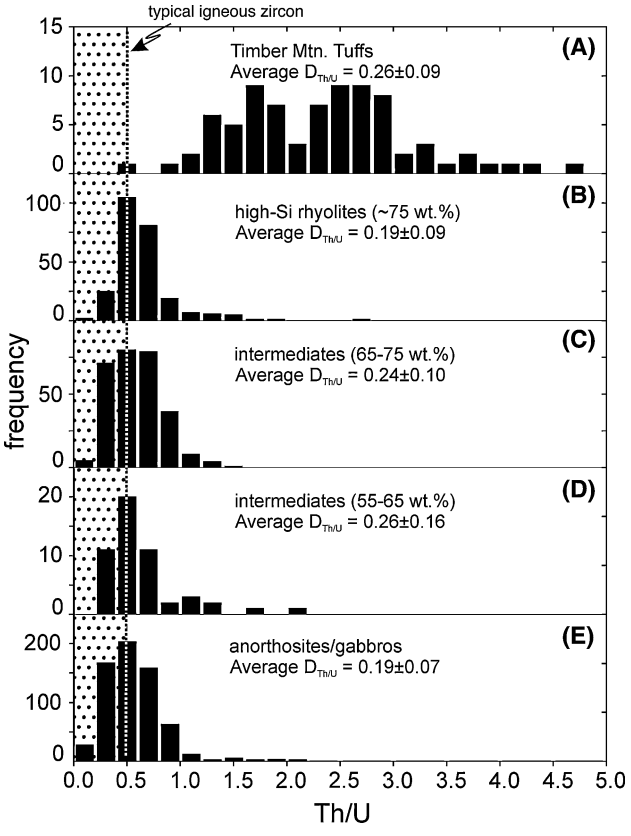

Fig. 7 A compilation of Th/U ratios in zircons and magmas from silicic igneous rocks with an emphasis on Cenozoic igneous rocks from the western USA (with the exception of **d** and **e**, which are for low-Si whole rock compositions including granodiorites, gabbroic anorthosites, and gabbros from MORB and intracontinental rift settings) in comparison to high Th/U ratios of Timber Mt latites and rhyolites. Note that $D_{Th/U}$ ratios calculated from literature whole-rock values are remarkably constant over a wide compositional and temperature range, suggesting a minor influence of these parameters on the relative partitioning behavior of Th and U in zircon. References: high silica rhyolites: Simon and Reid (2005), Vazquez and Reid (2002), Bindeman et al. (2001), Miller and Wooden (2004); intermediates (65–75 wt% SiO_2): Schmitt et al. (2003a, b), Bacon and Lowenstern (2005), Lowenstern et al. (2000); intermediates (55–65 wt% SiO_2): Schmitt et al. (2003a), Lowenstern et al. (2000), John et al. (2004); anorthosites/gabbros: Adirondack: McLelland et al. (2004), Duluth gabbroic anorthosite AS3 (unpublished data; this study) with calculated interstitial melt values from Grant and Chalokwu (1992), Black et al. (2004) and Southwest Indian Ridge gabbros from Schwartz et al. (2005)

Estimation of zircon inheritance proportion

The zircon saturation temperatures are on average 30°C higher than $\Delta^{18}O$(Qz-Mt) oxygen isotope equilibration temperatures and also higher than the Fe–Ti oxide equilibration temperatures (Fig. 9). Provided that the two latter temperatures reflect temperature of erupted magma, the higher temperature based on whole-rock Zr concentration may result from the excess zirconium due to zircon inheritance, or due to the presence of earlier crystallized zircons. Higher zircon saturation temperature is typical for many plutonic rocks, which segregated from metamorphic protoliths (e.g., Miller et al. 2003). An estimate can be made based on the Watson and Harrison (1983) zircon solubility equation for relevant peraluminous rhyolitic compositions at 700–850°C. This calculation suggests to us that 30°C higher temperature would result from ~100 ppm of additional Zr, which would correspond to 30–50% of the total zirconium (i.e. modal zircon) in the rock.

Discussion

Zircon inheritance, isotope zoning, and the origin of magmas in SWNVF

In order to better understand the significance of the U–Pb zircon ages, the results need to be considered in

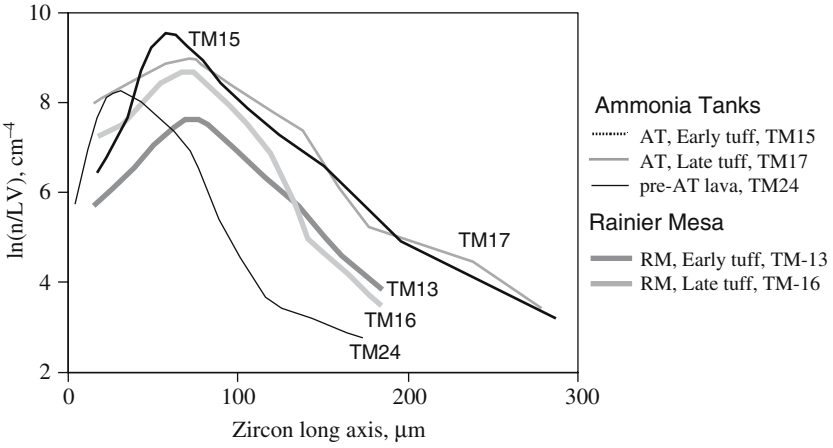

Fig. 8 Crystal size distribution of zircons from five samples in Timber Mt caldera complex: showing that zircons in AT tuff have both greater abundance and larger size than the RM tuff zircons, but similar modal abundance. Notice that zircons increase in abundance from pre-caldera to early, and then later tuffs. The pre-caldera lava sample TM-24 has a concave downward bend at ~100 μm interpreted to represent inherited larger grains. The lognormal shape is explained by annealing(s) of smaller zircons upon reheating, and/or subsequent size-dependent growth. The vertical axis plots logarithm population density in standard coordinates of number of crystals per unit volume (measured, Table 4), per bin size (10 μm)

Table 4 Abundance of quartz and zircon in Ammonia Tanks and Rainier mesa tuff units

		Zr (ppm WR)	Tsat (°C)	Crystals (%)	Quartz (%)	Zircon (ppmv)	Number of crystals/cm^3	
							Zircon	Quartz
Rainier mesa tuff								
TM-13	Early	97	757	16	4.9	7	47	
TM-16	Late	169	797	23	6.8	13	48	
Ammonia Tanks tuff and lavas								
TM-24	Pre-caldera	135	776	7	2.3	7	125	241
TM-17	Early	215	809	14	2.9	16	47	171
TM-15	Late	293	842	19	7.0	22	67	83
TM-21	Post-caldera	153	795	20	3.0			105

the petrological context of the SWNVF large-volume tuffs and lavas. Each tuff is characterized by a distinct range of $\delta^{18}O$ values, as well as distinct $^{87}Sr/^{86}Sr$ and ϵ_{Nd} values (Table 1 and Farmer et al. 1991), suggesting that the individual tuffs evolved separately, and that closed-system fractionation and assimilation in a single zoned, long-lived magma chamber is inconsistent with the observed isotopic heterogeneity. Instead, they represent independent large-volume magma batches that were generated on short timescales between successive caldera-forming eruptions. Furthermore, the isotopic and chemical differences between rhyolites and latites within individual eruptive sequences (Farmer et al. 1991; Mills et al. 1997; Bindeman and Valley 2003; Tefend 2005), including different $\delta^{18}O$, indicate that rhyolites and latites themselves represent distinct magma batches that could not be derived from each other by fractionation. Tefend (2005) and Tefend et al. (2006) further subdivided SWNVF rhyolites into low Th/Nb (0.5–0.8) and high Th/Nb (1.5–2) compositional groups. Indistinguishable $\delta^{18}O_{(Quartz)}$ in low and high Th/Nb rhyolites measured on these end member samples (Tefend and Bindeman, unpublished data) suggest, however, that these two types can be produced by accessory-mineral fractionation.

Zircon populations as a whole define ages that are significantly older than the eruption age. Without the petrological context outlined above, these zircon populations might have been interpreted as representing extended magma residence times on the order of a few million years. However, the isotopically distinct nature of each tuff unit, and especially oxygen isotopic zoning of zircons from the AT cycle, the presence of individual zircons that are much older (i.e., $> 2\sigma$, Fig. 5), and individual zircons with significantly higher $\delta^{18}O$ values (Fig. 6) indicate that they are ''inherited'' and variably

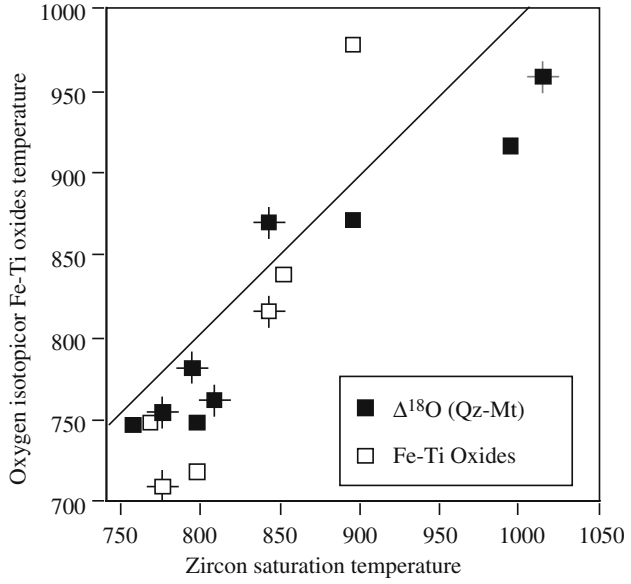

Fig. 9 Zircon saturation temperature (Watson and Harrison 1983) as compared to $\Delta^{18}O$(Qz-Mt) oxygen isotope temperature (Chiba et al. 1989) and Fe–Ti oxide temperature (Ghiorso and Sack 1991) for the same samples, data are from Bindeman and Valley (2003). Notice that zircon saturation temperature is higher by 30–50°C with the exception of two samples; *crosses* denote AT cycle magmas

equilibrated zircon populations. In this interpretation, the source magma cooled below its solidus, crystallized to develop open fractures, and was altered by hydrothermal circulation of meteoric waters, so the $\delta^{18}O$ of bulk rocks got depleted. Zircons, however, were unaffected, and preserved older inherited cores with higher $\delta^{18}O$ values. The voluminous low-$\delta^{18}O$ magmas of the AT cycle inherited their oxygen isotopic signature from the ^{18}O-depleted hydrothermally-altered rocks of the previous volcanic cycles (TS, TC, and RM). Based on the remaining $\Delta^{18}O$(Quartz–Zircon) and $\Delta^{18}O$(melt-zircon) disequilibria (Fig. 2b), and overlapping U–Pb zircon ages (Fig. 5), we concluded that the AT magma formed by remelting of hydrothermally-altered rocks of previous cycles only ~10 ka before its climactic eruption at 11.45 Ma (see Bindeman and Valley 2003). Zircon saturation temperatures of studied samples (Table 4), as well as $\Delta^{18}O$(Quartz–magnetite), and Fe–Ti oxide temperatures for the AT magmas are in the vicinity of 800°C, at the boundary of "cold" and "hot" granites (Miller et al. 2003). The survival of higher-$\delta^{18}O$ inherited cores in these samples additionally suggests that the heating pulse could not have lasted for longer than a few thousand years, based on the dissolution calculations by Watson (1996) for the dissolution of a typically sized zircon grain in peraluminous silicic melt upon reheating.

Experimental and empirical oxygen diffusion rates in zircon (Watson and Cherniak 1997; Peck et al. 2003) is seven to eight orders of magnitude slower than zirconium diffusion in melt, the rate-limiting step for zircon dissolution or crystallization (Harrison and Watson 1983). This suggests that during episodes of heating the zircon-melt boundary of a dissolving grain advances much faster towards the center of the grain than the oxygen diffusion front, as zircons are dissolving. Even if the increase in temperature upon reheating has resulted in initial dissolution of a certain fraction of inherited zircons, the surviving cores should have preserved their high-$\delta^{18}O$ cores. Examples of $\delta^{18}O$ preservation in inherited zircon cores are documented in migmatites (Page et al. 2006). Zircons will be preserved even better if they are armored in other phases, but we estimate the proportion of such zircons to be small (Bindeman 2003). Then, the surviving zircons were stored in the magma for several 1,000 years and developed isotopic zoning due to diffusion and overgrowth. In the case of multiple heating-reprecipitation cycles, this would still only recycle the outermost zircon layers that are in isotopic equilibrium, while leaving $\delta^{18}O$ in the cores relatively unchanged. Thus, upon dissolution, surviving zircons may preserve sharp boundaries with respect to oxygen isotopes; subsequent cooling episodes will lead to precipitation of new zircon rims, which are in oxygen isotopic equilibrium with respect to the host melt. In this case, $\delta^{18}O$ will show a step-function rather than bell-shaped profile will develop, but subsequent diffusive annealing may smooth it.

Precursor rhyolites in caldera settings

We observe that an AT cycle rhyolitic lava TM-24 contains zircons that are indistinguishable in age from those of the subsequent large-volume AT tuffs, and these zircons show similar patterns in oxygen isotopic heterogeneity (Fig. 2). The $^{40}Ar/^{39}Ar$ eruption age of the pre-AT rhyolite was not determined, but stratigraphic relations indicate that it shortly preceded the AT tuff. Chemically, isotopically, and mineralogically, the pre-AT lava closely matches the first erupted portions of the AT tuff (Table 1, Bindeman and Valley 2003; Farmer et al. 1991). Moreover, post-AT intracaldera lava (sample TM-21, Tables 1 and 4, not dated in this study) preserves the same character of isotopic zoning in zircons and $\Delta^{18}O$(Quartz–Zircon) and $\Delta^{18}O$(melt-zircon) disequilibria, as is observed in large volume AT tuffs, and TM-24 lava (Fig. 2). The timing of these two eruptions should therefore, be not much younger, or older, than the climactic caldera-forming eruption that produced AT tuff.

The identification of the pre-AT lava—sample TM-24—as a precursor volcanic unit contributes to the growing database of less voluminous lavas that often precede massive caldera-forming eruptions, such as the Pagosa Peak dacite that preceded the Fish Canyon tuff (Bachmann et al. 2000) or the Cleetwood lava that heralded the Mt Mazama eruption (Bacon 1983). Identification of these units may serve as petrological early-warning signal by providing an early sampling of a much larger magma body at depth.

Zircons as probes for crustal recycling

In recent years, extensive ion microprobe dating of zircon crystallization in volcanic samples complements traditional eruption age dating based on Ar–Ar and K–Ar methods. The underlying theme of these publications is that the zircon crystallization (and closure for subsequent U–Pb exchange) commonly predates the eruption of their host lavas as determined by the closure of the Ar–Ar system during cooling on the surface after eruption. This has been demonstrated for a range of differently sized magma systems, including Yellowstone as described above. Miller and Wooden (2004) found that zircons in Devils Kitchen rhyolite (Coso volcanic center, CA, USA) are up to 200 ky older than corresponding K–Ar ages, and several zircon populations with different pre-eruptive histories could be identified suggesting an origin from different magma batches. Simon and Reid (2005) suggested that zircons in the Glass Mountain rhyolites (Long Valley, CA, USA) record episodes of punctuated and independent evolution rather than the periodic tapping of a long-lived magma chamber. U–Pb zircon ages in combination with Ar–Ar potassium feldspar ages for the Geysers pluton (California Coast Ranges) indicate that the shallow portions of the pluton cooled to <350°C within ~200 ka, whereas at the same time zircons from just solidified granitoids at deeper levels became remobilized by the heat of newly intruded magma (Schmitt et al. 2003a, b). Charlier et al. (2003) found zircon ages spanning 100 ky in the Taupo volcanic zone in New Zealand, and interpreted zircons to be derived by bulk remobilization of crystal mush and assimilation of metasediment and/or silicic plutonic basement rocks. In their study of Crater Lake volcanic rocks, Bacon and Lowenstern (2005) succeeded in identifying and fingerprinting parental rocks as a source for antecrystic zircons and plagioclase in the form of co-erupted granodioritic blocks and magmas.

The conclusions that we reach here for the SWNVF support the emerging evidence for zircon recycling from earlier-intruded, solidified plutonic and subvolcanic rocks, or buried volcanic rocks, rather than ''long'' magma residence in large, long-lived magma reservoirs. However, the independent oxygen isotopic record for phenocrysts in the SVNVF, and the discovery of isotopically zoned zircons, allows us to further these interpretations and to discuss how large-volume silicic magmas could be generated so quickly.

Origin of high Th/U magmas

High Th/U ratios of Timber Mt zircons may yet present another evidence for hydrothermal alteration in the source region, because oxidizing meteoric water has a strong potential to mobilize U relative to Th during hydrothermal alteration (Sturchio et al. 1987). The high Th/U ratios of Timber Mt zircons corresponds to elevated Th/U ratios in SWNVF whole rocks (3 to 16, data extracted from a compilation by Warren et al. 2000), which result from moderately elevated Th (18–31 ppm), and moderately depleted (1–7 ppm) U concentrations. These Th/U ratios in Timber Mountain rocks are higher than median values for Th/U in basalts (3.5 ± 1.2; 1 standard deviation; n = 6061) and rhyodacites–rhyolites (median 3.9 ± 2.7; n = 695; data compiled from GEOROC-Geochemical Database http://www.georoc.mpch-mainz.gwdg.de/georoc/). Moreover, high and low Th/Nb groups identified by Mills et al. (1997) and Tefend (2005) in RM cycle magmas are correspondingly high Th/U and low Th/U, which also result from higher (lower) than average Th (U) concentrations. Because Timber Mountain zircons also preserve unusually high Th/U (Fig. 7) and are chemically inert during weathering, post-eruption U depletion can be ruled out as a cause for high Th/U in whole rocks. In the light of prolonged volcanism and hydrothermal activity in this area (since ~16 Ma, Christiansen et al. 1977), 4–3 million years long U removal via hydrothermal fluids in precursor intrusions or buried tuffs may instead explain high Th/U in Timber Mt. magmas. In this respect, it is interesting to compare Timber Mt with other areas of long-lived silicic caldera systems with associated hydrothermal activity. Low-δ^{18}O rhyolites from Yellowstone, for example, have Th/U between four and five (Sturchio et al. 1987), which is only slightly elevated compared to ''average'' rhyodacites–rhyolites. As another example, Taupo rhyolites have normal Th/U of ~4, but granitoid xenoliths in Taupo tuffs can reach Th/U of up to 30 (Charlier et al. 2005). Notably, some granitoid xenoliths from Taupo are also low in δ^{18}O (minimum + 1.7‰). In summary, while hydrothermal alteration by oxidizing fluids remains a potentially important mechanism for fractionating U and Th, alternative expla-

nations such as an imprint of pre-existing high Th/U crust via assimilation on the Timber Mt. magmas or accessory mineral fractionation in generation of high Th/Nb magmas (e.g., Tefend 2005) cannot be dismissed.

Implications for the generation and longevity of large silicic magma bodies

The formation of large silicic magma bodies is likely to occur by incremental addition of silicic portions formed either by differentiation of basaltic magmas in the crust, and/or by partial melting of the crust due to heat of basaltic intrusions (e.g., see Annen and Sparks 2002, and Dufek and Bergantz 2005 for a review of the current literature). Partial melting of the crust will very often generate isotopically-distinct individual magma batches. For example, Glass Mountain rhyolites, erupted over a time-span exceeding 1 Ma, exhibit heterogeneity with respect to Sr, Nd, Pb, and O isotopes between different domes (Davies and Halliday 1998; Bindeman and Valley 2002; Simon and Reid 2005). Subsequent accretion of such magma batches led to the formation of the Bishop tuff magma body, which averaged out isotopic differences in the melt, equilibrated $\delta^{18}O$ in minerals, and rejuvenated U–Pb age of zircons (Reid and Coath 2000), thus erasing the memory of smaller batch segregation. For example, zircons in individual pumice clasts from both late and early Bishop tuff are in perfect isotopic equilibrium at respective $\Delta^{18}O$(Qz-Mt) temperatures (Bindeman and Valley 2002) and lack any U–Pb evidence of inheritance from the Glass Mountain magmas (Simon and Reid 2005).

On the other end of the spectrum, Yellowstone intracaldera volcanic rocks are an example where almost the entire population of zircons is inherited from variable precaldera source rocks spanning 2 Myr (Bindeman et al. 2001). These rhyolites are the products of nearly wholesale remelting and recycling of hydrothermally-altered materials from earlier eruptive cycles, and they preserve extreme oxygen isotopic variability and zoning in phenocrysts, including quartz with relatively high diffusivity for oxygen (Bindeman and Valley 2001). This suggests that there was little time for isotopic exchange between melting and eruption. Large-volume ignimbrites of Yellowstone are much more homogeneous.

An obvious difference between Yellowstone and SWNVF is that the recurrence intervals between large-volume eruptions was shorter for the SWNVF: in the case of Rainier Mesa and AT the recurrence interval was only ~150 ka, as compared to ~700 ka between the two last caldera-forming eruptions at Yellowstone (Mesa Falls Tuff and Lava Creek Tuff). There is also a possibility that extensional tectonic settings of the Basin and Range at SWNVF caused different styles of magma ascent and emplacement. It appears that within the SWNVF, individual, isotopically-distinct melt batches with variable $\delta^{18}O$ zircons (Fig. 6) generated by reheating of hydrothermally-altered rocks were able to coalesce into a ~1,000 km^3 size magma body. It is remarkable, however, that neither different parts of this large magma body, exemplified by the study of individual pumice clasts dispersed by the caldera-forming eruptions (Mills at al. 1997; Tefend 2005), nor crystal populations, exemplified by this study of AT cycle magmas, achieved isotopic equilibration.

The short magma segregation time for low-$\delta^{18}O$ AT cycle magmas is the time to melt and digest hundreds of cubic kilometers of hydrothermally-altered low-$\delta^{18}O$ protolith, and inherit zircons with older ages and higher-$\delta^{18}O$ cores. High magma production rates require intrusion of substantial volumes of basaltic magmas on the order of several hundreds of km^3, that could preceded the melting process. Intrusion and differentiation of basaltic magma prior to melting/assimilation of the shallow low-$\delta^{18}O$ crust could have taken longer. Thermomechanical modeling by Annen and Sparks (2002) and Dufek and Bergantz (2005) implies that a series of small intrusions closely clustering in space and time, rather than a single episode of intrusion of a thick basaltic sill is the preferred mechanism both from the perspective of heat and space conservation. Rapid, nearly whole-sale melting of shallow crust presents a significant challenge to melting scenarios by basaltic underplating.

Results presented here for the SWNVF are consistent with melting at shallow crustal level where meteoric water percolated, i.e. most likely at depths < 10 km, or potentially only a few kilometers. Such shallow levels raise the question: how is space created for large and shallow magma chambers? Cambray et al. (1995) and Vogel et al. (2001) suggested that extensional tectonics in the Basin and Range produces ''releasing steps'' in normal dip–slip detachment faults that then can serve as magma traps. These magma traps may expand with further extension and can accommodate further influxes of magma, thus forming sheet-like large-volume magma bodies by incremental addition. Furthermore, this tectonic framework creates conditions for shallow-level generation of magma bodies, and the spatial separation of isotopically discrete magma batches.

We propose that hydrothermally-altered intra-caldera crustal segments are heated following significant

(ca. 1–4 km) vertical down-drop associated with each caldera collapse. Furthermore, complex geometry of collapsed blocks (e.g., Lipman 1997) can be expected, causing faster temperature increase and preferential melting in sheets, slivers and corners. Heat-flow calculations using the HEAT software (Ken Wohletz; http://www.ees1.lanl.gov/Wohletz/Heat.htm) suggest that a collapsed block immersed into the hot interior of a magma chamber will melt ~3–5 times faster than by unidirectional heat conduction as in the case of magmatic underplating. Bulk digestion process starts when interstitial melt forms an interconnected network, causing the roof rock to collapse and to disintegrate into individual phenocrysts or crystal clusters (Bacon and Lowenstern 2005; Beard et al. 2005). The resulting crystal mush then collapses and becomes homogenized by convection. This process may generate chemical and isotopic differences between the crystal poorer rhyolites, and crystal-richer latites. Magmatic overgrowth, and isotopic diffusion and re-equilibration of crystals will last until the time of eruptive quench.

Acknowledgments This research was supported by the University of Oregon, US Department of Energy under grant FGO2-93ER14389, DOE/NV/14389-2001-1). We thank IF-EAR program of the NSF for support of the ion microprobe facilities at UCLA and UW-Madison. Tom Vogel and Jake Lowenstern are thanked for thoughtful reviews.

References

Annen C, Sparks RSJ (2002) Effects of repetitive emplacement of basaltic intrusions on thermal evolution and melt generation in the crust. Earth Planet Sci Lett 203:937–955

Bachmann O, Bergantz GW (2003) Rejuvenation of the Fish Canyon magma body: a window into the evolution of large-volume silicic magma systems. Geology 31:789–792

Bachmann O, Bergantz GW (2004) On the origin of crystal-poor rhyolites: extracted from Batholithic crystal mushes. J Petrol 45:1565–1582

Bachmann O, Dungan MA , Lipman PW (2000) Voluminous lava-like precursor to a major ash-flow tuff: low-column pyroclastic eruption of the Pagosa Peak Dacite San Juan volcanic field Colorado. J Volcanol Geotherm Res 98:153–171

Bacon CR (1983) Eruptive history of mount Mazama and Crater Lake caldera Cascade Range USA. J Volcanol Geotherm Res 18(1–4):57–115

Bacon CR, Lowenstern JB (2005) Late Pleistocene granodiorite source for recycled zircon and phenocrysts in rhyodacite lava at Crater Lake Oregon. Earth Planet Sci Lett 233:277–293

Beard JS, Ragland PC, Crawford ML (2005) Reactive bulk assimilation: a model for crust-mantle mixing in silicic magmas. Geology 33:681–684

Bindeman IN (2003) Crystal sizes in evolving silicic magma chambers. Geology 31:367–370

Bindeman IN, Valley JW (2001) Low-δ^{18}O rhyolites from Yellowstone: magmatic evolution based on analyses of zircons and individual phenocrysts. J Petrol 42:1491–1517

Bindeman IN, Valley JW (2002) Oxygen isotope study of Long-Valley magma system: isotope thermometry and role of convection. Contrib Mineral Petrol 144:185–205

Bindeman IN, Valley JW (2003) Rapid generation of both high- and low-delta O-18 large-volume silicic magmas at the Timber Mountain/Oasis Valley caldera complex Nevada. Geol Soc Am Bull 115:581–595

Bindeman IN, Valley JW, Wooden JL, Persing HM (2001) Post-caldera volcanism: in situ measurement of U–Pb age and oxygen isotope ratio in Pleistocene zircons from Yellowstone caldera. Earth Planet Sci Lett 189:197–206

Bindeman IN, Sigmarsson O, Eiler J (2006) Time constraints on the origin of large volume basalts derived from O-isotope and trace element mineral zoning and U-series disequilibria in the Laki and Grimsvotn volcanic system. Earth Planet Sci Lett 245(1–2):245–259

Black LP, Kamo SL, Allen CM, Aleinikoff JN, Davis DW, Korsch RJ, Foudoulis C (2004) TEMORA 1: a new zircon standard for Phanerozoic U–Pb geochronology. Chem Geol 200:155–170

Blundy J, Wood B (2003) Mineral-melt partitioning of uranium thorium and their daughters. In: Bourdon B, Henderson GM, Lundstrom CC, Turner SP (eds) Uranium-series geochemistry. Rev Mineral Geochem 52: 59–123

Boroughs S, Wolff J, Bonnichsen B, Godchaux M, Larson P (2005) Large-volume, low-delta O-18 rhyolites of the central Snake River Plain, Idaho, USA. Geology 33:821–824

Broxton DE, Warren RG, Byers FM Jr, Scott RB (1989) Chemical and mineralogic trends within the Timber Mountain-Oasis Valley caldera complex NV: evidence for multiple cycles of chemical evolution in a long-lived silicic magma system. J Geophys Res 94:5961–5985

Byers FM Jr, Carr WJ, Christiansen RL, Lipman PW, Orkild PP, Quinlivan WD (1976a) Volcanic suites and related cauldrons of Timber Mountain-Oasis valley caldera complex Southern Nevada. US Geological Survey Professional Paper 919:71

Byers FM Jr, Carr WJ, Orkild PP, Quinlivan WD, Sargent KA (1976b) Geologic map of the Timber Mountain caldera area Nye county Nevada US Geological Survey Miscellaneous Investigations Series: Map I-891 1 sheet

Byers FM Jr, Carr WJ, Orkild PP (1989) Volcanic centers of south-western Nevada: evolution of understanding (1960–1988). J Geophys Res 94:5908–5924

Cambray FW, Vogel TA, Mills JG Jr (1995) Origin of compositional heterogeneities in tuffs of the Timber Mountain Group: the relationship between magma batches and magma transfer and emplacement in an extensional environment. J Geophys Res 100(B8):15793–15805

Compston W, Williams IS, Meyer C (1984) U–Pb geochronology of zircons from lunar breccia 73217 using a sensitive high mass-resolution ion microprobe. J Geophys Res 89:B525–B534

Costa F, Chakraborty S, Dohmen R (2003) Diffusion coupling between trace and major elements and a model for calculation of magma residence times using plagioclase. Geochim Cosmochim Acta 67:2189–2200

Charlier BLA, Peate PW, Wilson CJN, Lowenstern JB, Storey M, Brown SJA (2003) Crystallisation ages in coeval silicic magma bodies: ^{238}U–^{230}Th disequilibrium evidence from the Rotoiti and Earthquake Flat eruption deposits, Taupo Volcanic Zone, New Zealand. Earth Planet Sci Lett 206:441–457

Charlier BLA, Wilson CJN, Lowenstern JB, Blake S, Van Calsteren PW, Davidson JP (2005) Magma generation at a large hyperactive silicic volcano (Taupo New Zealand) revealed by U–Th and U–Pb systematics in zircons. J Petrol 46(1):3–32

Christiansen RL, Lipman PW, Carr WJ, Byers FM Jr, Orkild PP, Sargent KA (1977) Timber Mountain-Oasis Valley caldera complex of southern Nevada. Geol Soc Am Bull 88:943–959

Crank J (1975) The mathematics of diffusion 2nd edn Oxford University Press

Davies GR, Halliday AN (1998) Development of the Long Valley rhyolitic magma system: Sr and Nd isotope evidence from glasses and individual phenocrysts. Geochim Cosmochim Acta 62:3561–3574

Dufek J, Bergantz GW (2005) Lower crustal magma genesis and preservation: a stochastic framework for the evaluation of basalt–crust interaction. J Petrol 46:2167–2195

Eaton GP (1984) The Miocene Great Basin of western North America as an extending back-arc region. In: Carlson RL and Kobayashi K (eds) Geodynamics of back-arc regions. Tectonophys 102:275–295

Farmer GL, Broxton DE, Warren RG, Pickthorn W (1991) Nd Sr and O isotopic variations in metaluminous ash-flow tuffs and related volcanic rocks at the Timber Mountain/Oasis Valley Caldera Complex SW Nevada: implications for the origin and evolution of large-volume silicic magma bodies. Contrib Mineral Petrol 109:53–68

Flood TP, Vogel TA, Schuraytz BC (1989) Chemical evolution of a magmatic system: the Paintbrush Tuff SW Nevada volcanic field. J Geophys Res 94:5943–5960

Friedman I, Lipman PW, Obradovich JD, Gleason JD, Christiansen RL (1974) Meteoric water in magmas. Science 184:1069–1072

Ghiorso MS, Sack RO (1991) Fe–Ti oxide geothermometry-thermodynamic formulation and the estimation of intensive variables in silicic magmas. Contrib Mineral Petrol 108:485–510

Grant NK, Chalokwu CI (1992) Petrology of the Partridge River Intrusion Duluth Complex Minnesota; II Geochemistry and strontium isotope systematics in Drill Core DDH-221. J Petrol 33:1007–1038

Hildreth W, Christiansen RL, O'Neil JR (1984) Catastrophic isotopic modification of rhyolitic magma at times of caldera subsidence, Yellowstone Plateau Volcanic Field. J Geophys Res 89:8339–8369

Hildreth W, Halliday AN, Christiansen RL (1991) Isotopic and chemical evidence concerning the genesis and contamination of basaltic and rhyolitic magmas beneath the Yellowstone Plateau Volcanic Field. J Petrol 32:63–138

Hoskin PWO, Schaltegger U (2003) The composition of zircon and igneous and metamorphic petrogenesis In: Hanchar JM, Hoskin PWO (eds) Zircon. Rev Mineral Geochem 53:27–62

Huysken KT, Vogel TA, Layer PW (1994) Incremental growth of a large-volume chemically zoned magma body—a study of the tephra sequence beneath the Rainier Mesa ash-flow sheet of the Timber Mountain Tuff. Bull Volcanol 56:377–385

Huysken KT, Vogel TA, Layer PW (2001) Tephra sequences as indicators of magma evolution: Ar-40/Ar-39 ages and geochemistry of tephra sequences in the southwest Nevada volcanic field. J Volcanol Geotherm Res 106:85–110

John BE, Foster DA, Murphy JM, Cheadle MJ, Baines AG, Mark Fanning C, Copeland P (2004) Determining the cooling history of in situ lower oceanic crust—Atlantis Bank, SW Indian Ridge. Earth Planet Sci Lett 222:145–160

Lipman PW (1971) Iron–titanium oxide phenocrysts in compositionally zoned ash-flow sheets from southern Nevada. J Geology 79:438–456

Lipman PW (1984) The roots of ash-flow calderas in the western North America: windows into the tops of granitic batholiths. J Geophys Res 89:8801–8841

Lipman PW (1997) Subsidence of ash-flow calderas: relation to caldera size and magma-chamber geometry. Bull Volcanol 59:198–218

Lipman PW, Friedman I (1975) Interaction of meteoric water with magmas: an oxygen isotope study of ash-flow sheets from southern Nevada. Geol Soc Am Bull 86:695–702

Lipman PW, Christiansen RL, O'Connor JT (1966) A compositionally-zoned ash-flow sheet in southern Nevada. US Geological Survey Professional Paper 524-F:1–47

Lipman PW, Protska HJ, Christiansen RL (1972) Cenozoic volcanism and plate tectonic evolution of the western United States; I Early and middle Cenozoic. R Soc Lond Phil Trans A 271:217–248

Lowenstern JB, Persing HM, Wooden JL, Lanphere M, Donnelly-Nolan J, Grove TL (2000) U–Th dating of single zircons from young granitoid xenoliths: new tools for understanding volcanic processes. Earth Planet Sci Lett 183:291–302

Mahon K (1996) The New 'York' regression: application of an improved statistical method to geochemistry. Int Geol Rev 38:293–303

McLelland JM, Bickford ME, Hill BM, Clechenko CC, Valley JW, Hamilton MA (2004) Direct dating of Adirondack massif anorthosite by U–Pb SHRIMP analysis of igneous zircon: implications for AMCG complexes. Geol Soc Am Bull 116:1299–1317

Miller JS, Wooden JL (2004) Residence Resorption and Recycling of Zircons in Devils Kitchen Rhyolite Coso Volcanic Field, California. J Petrol 45:2155–2170

Miller CF, McDowell SM, Mapes RW (2003) Hot and cold granites? Implications of zircon saturation temperatures and preservation of inheritance. Geology 31(6):529–532

Mills JG Jr, Saltoun BW, Vogel TA (1997) Magma batches in the Timber Mountain magmatic system SW Nevada volcanic field Nevada, USA. J Volcanol Geotherm Res 78:185–208

Paces JB, Miller JD (1993) Precise U–Pb ages of Duluth Complex and related mafic intrusions northeastern Minnesota; geochronological insights to physical petrogenetic paleomagnetic and tectonomagnetic processes associated with the 11 Ga midcontinent rift system. J Geophys Res 98:13997–14013

Page Z, DeAngelis M, Fu B, Kita N, Lancaster PJ, Valley JW (2006) Slow oxygen diffusion in zircon. Goldschmidt Abstract (in press)

Peck WH, Valley JW, Graham CM (2003) Slow oxygen diffusion rates in igneous zircons from metamorphic rocks. Am Mineral 88:1003–1014

Poldervaart A (1956) Zircon in rocks: 2. Igneous rocks. Am J Sci 254:521–554

Reid MR, Coath CD (2000) In situ U–Pb ages of zircons from the Bishop Tuff: no evidence for long crystal residence times. Geology 28:443–446

Reid MR, Coath CD, Harrison MT, McKeegan KD (1997) Prolonged residence times for the youngest rhyolites associated with Long Valley caldera: ^{230}Th–^{238}U ion microprobe dating of young zircons. Earth Planet Sci Lett 150:27–39

Sawyer DA, Fleck RJ, Lanphere MA, Warren RG, Broxton DE, Hudson MR (1994) Episodic caldera volcanism in the Miocene SW Nevada volcanic field: related stratigraphic framework ^{40}Ar/^{39}Ar geochronology and implications for magmatism and extension. Geol Soc Am Bull 106:1304–1318

Schärer U (1984) The effect of initial 230Th disequilibrium on young U–Pb ages: the Makalu case Himalaya. Earth Planet Sci Lett 67:191–204

Schmitt AK, Grove M, Harrison TM, Lovera O, Hulen JB, Walters M (2003a) The Geysers-Cobb mountain magma system California (Part 1): U–Pb zircon ages of volcanic rocks conditions of zircon crystallization and magma residence times. Geochim Cosmochim Acta 67:3423–3442

Schmitt AK, Grove M, Harrison TM, Lovera O, Hulen JB, Walters M (2003b) The Geysers-Cobb mountain magma system California (Part 2): timescales of pluton emplacement and implications for its thermal history. Geochim Cosmochim Acta 67:3443–3458

Schuraytz BC, Vogel TA, Younker LW (1989) The Topopah Spring Tuff: evidence for dynamic withdrawal from a layered magma body. J Geophys Res 94:5925–5942

Schwartz JJ, John BE, Cheadle MJ, Miranda EA, Grimes GB, Wooden JL, Dick HJB (2005) Dating the growth of oceanic crust at a slow-spreading Ridge. Science 310:654–657

Simon JI, Reid MR (2005) The pace of rhyolite differentiation and storage in an 'archetypical' silicic magma system Long Valley. Earth Planet Sci Lett 235:123–140

Sturchio NC, Binz CM, Lewis CH III (1987) Thorium–uranium disequilibrium in a geothermal discharge zone at Yellowstone. Geochim Cosmochim Acta 51:2025–2034

Tefend KS (2005) Independently generated magma batches in the compositionally zoned ash-flow sheets from the southwest Nevada volcanic field. Ph.D. dissertation, Michigan State University, East Lansing

Tefend KS, Vogel TA, Flood TP, Ehrlich R (2006) Identifying relationships among Silicic magma batches by polytopic vector analysis: a study of the Topopah Spring and Pah Canyon ash-flow sheets of the southwest Nevada volcanic field. J Volcanol Geotherm Res (in press)

Tepley FJ, Davidson JP (2003) Mineral-scale Sr-isotope constraints on magma evolution and chamber dynamics in the Rum layered intrusion, Scotland. Contrib Mineral Petrol 145:628–641

Tepley FJ, Davidson JP, Clynne MA (1999) Magmatic interactions as recorded in plagioclase phenocrysts of Chaos Crags, Lassen Volcanic Center, California. J Petrol 40:787–806

Valley JW (2003) Oxygen isotopes in zircon. Rev Mineral Geochem 53: 343–385

Valley JW, Bindeman IN, Peck WH (2003) Empirical calibration of oxygen isotope fractionations in zircon. Geochim Cosmochim Acta 67:3257–3266

Valley JW, Lackey JS, Cavosie AJ, Clechenko CC, Spicuzza MJ, Basei MAS, Bindeman IN, Ferreira VP, Sial AN, King EM, Peck WH, Sinha AK, Wei CS (2005) 4.4 billion years of crustal maturation: oxygen isotopes in magmatic zircon. Contrib Mineral Petrol 150:561–580

Vazquez JA, Reid MR (2002) Time scales of magma storage and differentiation of voluminous high-silica rhyolites at Yellowstone caldera, Wyoming. Contrib Mineral Petrol 144:274–285

Vogel TA, Aines R (1996) Melt inclusions from chemically zoned ash-flow sheets from the Southwest Nevada volcanic field. J Geophys Res 101:5591–5610

Vogel TA, Cambray FW, Constenius KN (2001) Origin and emplacement of igneous rocks in the central Wasatch Mountains, Utah. Rocky Mt Geol 36:119–162

Warren RG, Byers FM Jr, Broxton DE, Freeman SH, Hagan RC (1989) Phenocrysts abundances and glass and phenocrysts compositions as indicator of magmatic environments of large volume ash-flow sheets in southwestern Nevada. J Geophys Res 94:5987–6020

Warren RG, Sawyer DA, Byers FM Jr, Cole GL (2000) A petrographic/geochemical database and stratigraphic framework for the southern Nevada volcanic field. Los Alamos Report http://www.pggdb-swnvf.lanl.gov/report/database.html

Watson EB (1996) Dissolution, growth and survival of zircons during crustal fusion: kinetic principles, geological models and implications for isotopic inheritance. Trans R Soc Edinb Earth Sci 87:43–56

Watson EB, Harrison TM (1983) Zircon saturation revisited: temperature and compositional effects in a variety of crustal magma types. Earth Planet Sci Lett 64:295–304

Watson EB, Cherniak DJ (1997) Oxygen diffusion in zircon. Earth Planet Sci Lett 148:527–544

Wendt I, Carl C (1985) U/Pb dating of discordant 01 Ma old secondary U minerals. Earth Planet Sci Lett 73:278–284

Wolff JA, Ramos FC (2003) Pb isotope variations among Bandelier Tufffeldspars: no evidence for a long-lived silicic magma chamber. Geology 31:533–536

Wiedenbeck M, Alle P, Corfu F, Griffin WL, Meier M, Oberli F, Von Quadt A, Roddick JC, Spiegel W (1995) Three natural zircon standards for U–Th–Pb Lu–Hf trace element and REE analyses. Geostandards Newslett 91:1–23

Wiedenbeck M, Hanchar JM, Peck WH, Sylvester P, Valley J, Whitehouse M, Kronz A, Morishita Y, Nasdala L, Fiebig J, Franchi I, Girard JP, Greenwood RC, Hinton R, Kita N, Mason PRD, Norman M, Ogasawara M, Piccoli R, Rhede D, Satoh H, Schulz-Dobrick B, Skar O, Spicuzza MJ, Terada K, Tindle A, Togashi S, Vennemann T, Xie Q, Zheng YF (2004) Further characterisation of the 91500 zircon crystal. Geostand Geoanal Res 28(1):9–39